J. Appl. Comput. Mech., 8(1) (2022) 370-378
DOI: 10.22055/JACM.2021.37953.3141

ISSN: 2383-4536
jacm.scu.ac.ir

Shahid Chamran University of Ahvaz

Journal of Applied and Computational Mechanics

Research Paper

Effects of Periodic Loading on Longitudinal Fracture in Viscoelastic Functionally Graded Beam Structures

Victor Rizov

Department of Technical Mechanics, University of Architecture, Civil Engineering and Geodesy, 1 Chr. Smirnensky blvd., Sofia, 1046, Bulgaria

Received July 27 2021; Revised September 17 2021; Accepted for publication November 26 2021.
Corresponding author: V. Rizov (v_rizov_fhe@uacg.bg)

Abstract. This paper analyzes the effects of periodic external loading on the longitudinal fracture of a beam structure made of linear viscoelastic material. A longitudinal crack splits the cracked part of the beam into left-hand and right-hand crack arms. The beam is under a bending moment applied at the free end of the right-hand crack arm. The bending moment varies periodically with time. The material of the beam is continuously inhomogeneous (functionally graded) along the thickness. Thus, the modulus of elasticity and the coefficient of viscosity of the material vary continuously in transversal direction of the beam. The balance of the energy in the beam under periodic bending moment is analyzed in order to derive the strain energy release rate for the longitudinal crack. The solution is verified by deriving the strain energy release rate by analyzing of the compliance of the beam subjected to periodic bending moment. An investigation is carried-out by applying the solutions obtained in order to evaluate the effects of the parameters of the periodic loading on the strain energy release rate.

Keywords: Viscoelastic beam, Inhomogeneous material, Longitudinal fracture, Functionally graded structure, Periodic loading.

1. Introduction

The aspiration for improving the efficiency of engineering structures and facilities necessitates quest for new technical decisions and use of modern structural materials. In this relation, a very good alternative of the conventional homogeneous materials are the continuously inhomogeneous materials with location-dependent mechanical properties. Since their properties vary smoothly along one or more coordinates in a structural component, there are no discernible internal boundaries and interfaces between different constituent materials which is one the important advantages of continuously inhomogeneous materials over the fiber reinforced composites. One of the most widely used types of continuously inhomogeneous materials that have received considerable attention worldwide in the recent decades is the functionally graded materials [1-6]. The mechanical properties of functionally graded materials are specially adjusted by gradually varying the microstructure and composition of their constituent materials during manufacturing to meet the performance requirements [7-13].

Various load-bearing engineering structures and their components are always confronted with problems of integrity and reliability. Therefore, ensuring of safety and durability of continuously inhomogeneous structures is a constant aim and challenge to engineers in the design process. Fracture is one of the most frequent and dangerous type of failure of constructions. Especially for continuously inhomogeneous (functionally graded) beam structures, the longitudinal fracture is a problem of significant importance since these structures can be build-up layer by layer which is a cause for appearance of cracks between layers [14]. Thus, analyses of longitudinal fracture play a decisive role in design of safe and reliable beam structures [15-17].

Under certain conditions, structural materials exhibit linear viscoelastic behaviour, i.e. they deform in time keeping linear dependence between stresses and strains. For load-bearing structures made of continuously inhomogeneous materials, the viscoelastic behaviour is of substantial importance. The viscoelastic properties of structural members and components have significant influence on reliability of the structures. Therefore, neglecting the viscoelastic behaviour can affect the functioning of continuously inhomogeneous engineering structures and even can lead to structural collapse.

The aim of this paper is to analyze the longitudinal fracture in a linear viscoelastic beam structure under a bending moment that varies periodically with time. The beam is made of continuously inhomogeneous (functionally graded) material. In many instances, the inhomogeneous viscoelastic beams are under periodic external loading. Because of this, it is important to develop analyses of longitudinal fracture of such beams under periodic loading. The previous studies deal usually with longitudinal fracture of inhomogeneous viscoelastic beams subjected to constant loading [18-20]. This fact emphasizes the need of analyses which take into account periodic change of the loading. In this paper, the strain energy release rate under periodic bending moment is obtained by analyzing the balance of the energy. The compliance method is applied for verification of the strain energy release rate. The effects of the parameters of the periodic loading on the strain energy release rate are evaluated. It can be indicated that the innovation of this paper is that the analysis of longitudinal fracture takes into account the viscoelastic behaviour of continuously inhomogeneous (functionally graded) beam structure under periodical loading.

Published online: November 28 2021

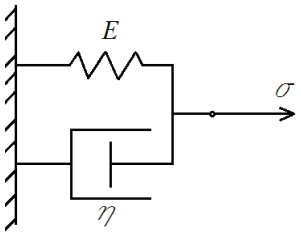

Fig. 1. Viscoelastic model.

2. Deriving of the Strain Energy Release Rate

The viscoelastic model depicted in Fig. 1 is made up by a linear spring placed in parallel to a linear dashpot. The spring and the dashpot are characterized by modulus of elasticity, E, and coefficient of viscosity, η, respectively. The model is known as the Voigt-Kelvin linear viscoelastic mechanical model. In this paper, the model is subjected to a stress, σ, that varies periodically with time, t, as depicted in Fig. 2. At

$$t_i \le t \le t_i + T_\alpha , \tag{1}$$

$$\sigma = \sigma_\alpha . \tag{2}$$

at

$$t_i + T_\alpha \le t \le t_i + T_\alpha + T_\beta , \tag{3}$$

$$\sigma = \sigma_\beta , \tag{4}$$

where

$$\sigma_\beta = \beta \sigma_\alpha , \tag{5}$$

$$T_\alpha = fT , \tag{6}$$

$$T_\beta = (1-f)T , \tag{7}$$

$$0 < f < 1 . \tag{8}$$

Here, T is the period of the stress (Fig. 2).

The strain in the model is derived by using the following equation of equilibrium:

$$\sigma_\eta + \sigma_E = \sigma \tag{9}$$

where σ_η and σ_E are the stresses in the dashpot and the spring, respectively. These stresses are obtained as

$$\sigma_\eta = \eta \dot{\varepsilon} , \tag{10}$$

$$\sigma_E = E\varepsilon , \tag{11}$$

where ε is the strain.

The first derivative of the strain with respect to time is designated by $\dot{\varepsilon}$. By substituting of (10) and (11) in (9), one derives the following inhomogeneous differential equation:

$$\dot{\varepsilon} + \delta\varepsilon = \frac{\sigma}{\eta} , \tag{12}$$

where

$$\delta = \frac{E}{\eta} . \tag{13}$$

The solution of (11) is written as

$$\varepsilon = C_1 e^{-\delta t} + \bar{\varepsilon} , \tag{14}$$

where C_1 is an interactional constant, $\bar{\varepsilon}$ is a particular solution of (11). The term, $C_1 e^{-\delta t}$, in (14) quickly approaches zero with increasing of t. Therefore, this term can be neglected and the strain in the model is written as

$$\varepsilon = \bar{\varepsilon} . \tag{15}$$

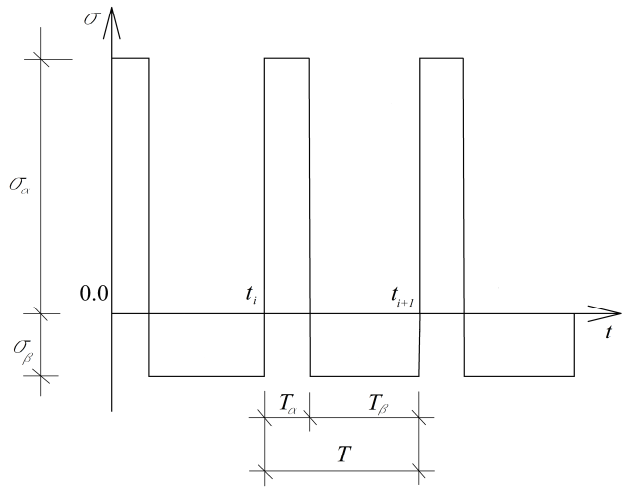

Fig. 2. Variation of the stress with time.

In order to obtain the particular solution, $\bar{\varepsilon}$, the stress is expanded in series of Fourier

$$\sigma = B_0 + \sum_{j=1}^{\infty} B_j \cos(j\bar{\omega}t) + \sum_{j=1}^{\infty} D_j \sin(j\bar{\omega}t), \tag{16}$$

where

$$\bar{\omega} = \frac{2\pi}{T}. \tag{17}$$

The coefficients in the series of Fourier are expressed as

$$B_0 = \frac{1}{T}\int_0^T \sigma(t)dt = \frac{1}{T}\left[\int_0^{T_\alpha} \sigma_\alpha dt + \int_{T_\alpha}^{T} \sigma_\beta dt\right], \tag{18}$$

$$B_j = \frac{2}{T}\int_0^T \sigma(t)\cos(j\bar{\omega}t)dt = \frac{2}{T}\left[\int_0^{T_\alpha} \sigma_\alpha \cos(j\bar{\omega}t)dt + \int_{T_\alpha}^{T} \sigma_\beta \cos(j\bar{\omega}t)dt\right], \tag{19}$$

$$D_j = \frac{2}{T}\int_0^T \sigma(t)\sin(j\bar{\omega}t)dt = \frac{2}{T}\left[\int_0^{T_\alpha} \sigma_\alpha \sin(j\bar{\omega}t)dt + \int_{T_\alpha}^{T} \sigma_\beta \sin(j\bar{\omega}t)dt\right], \tag{20}$$

$$B_0 = \sigma_\alpha\left[f + \beta(1-f)\right]. \tag{21}$$

After substituting of (5), (6) and (7) in (18), (19) and (20), one obtains

$$B_j = \frac{2\sigma_\alpha}{Tj\bar{\omega}}\left\{\sin(j\bar{\omega}fT) + \beta\left[\sin(j\bar{\omega}T) - \sin(j\bar{\omega}fT)\right]\right\}, \tag{22}$$

$$D_j = \frac{2\sigma_\alpha}{Tj\bar{\omega}}\left\{1 - \cos(j\bar{\omega}fT) + \beta\left[\cos(j\bar{\omega}fT) - \cos(j\bar{\omega}T)\right]\right\}. \tag{23}$$

Since the stress in the right-hand side of equation (12 is expressed in the form (17), the particular solution of (12) is written as

$$\bar{\varepsilon} = Q_0 + \sum_{j=1}^{\infty} P_j \cos(j\bar{\omega}t) + \sum_{j=1}^{\infty} R_j \sin(j\bar{\omega}t). \tag{24}$$

The quantities, Q_0, P_j and R_j, are obtained in the following way. First, the derivative of (24) with respect to time is found as

$$\dot{\bar{\varepsilon}} = -\sum_{j=1}^{\infty} P_j j\bar{\omega}\sin(j\bar{\omega}t) + \sum_{j=1}^{\infty} R_j j\bar{\omega}\cos(j\bar{\omega}t). \tag{25}$$

By substituting of (16), (24) and (25) in (12), one obtains

$$-\sum_{j=1}^{\infty} P_j j\bar{\omega}\sin(j\bar{\omega}t) + \sum_{j=1}^{\infty} R_j j\bar{\omega}\cos(j\bar{\omega}t) + \delta\left[\ Q_0 + \sum_{j=1}^{\infty} P_j \cos(j\bar{\omega}t) + \sum_{j=1}^{\infty} R_j \sin(j\bar{\omega}t)\ \right] + Q\delta = \frac{B_0}{\eta} + \sum_{j=1}^{\infty} \lambda_j \cos(j\bar{\omega}t) + \sum_{j=1}^{\infty} \mu_j \sin(j\bar{\omega}t) \tag{26}$$

where

$$\lambda_j = \frac{B_j}{\eta}. \tag{27}$$

$$\mu_j = \frac{D_j}{\eta}. \tag{28}$$

By equalizing of $Q\delta$ and B_0 / η, one derives

$$Q = \frac{B_0}{E}. \tag{29}$$

Then, by equalizing of the coefficients of $\cos(j\bar{\omega}t)$ and $\sin(j\bar{\omega}t)$, respectively, one obtains

$$-P_j j\bar{\omega} + \delta_j R_j = \mu_j, \tag{30}$$

$$R_j j\bar{\omega} + \delta P_j = \lambda_j, \tag{31}$$

Equations (30) and (31) are solved with respect to P_j and R_j. The result is

$$P_j = \frac{\delta\lambda_j - \mu_j j\bar{\omega}}{j^2\bar{\omega}^2 + \delta^2}, \tag{32}$$

$$R_j = \frac{\mu_j}{\delta} + \frac{\left(\delta\lambda_j - \mu_j j\bar{\omega}\right) j\bar{\omega}}{\delta\left(j^2\bar{\omega}^2 + \delta^2\right)}. \tag{33}$$

By substituting of (24) and (29) in (15), one derives

$$\varepsilon = \frac{B_0}{E} + \sum_{j=1}^{\infty} P_j \cos(j\bar{\omega}t) + \sum_{j=1}^{\infty} R_j \sin(j\bar{\omega}t), \tag{34}$$

where P_j and R_j are found by (32) and (33), respectively. By using (17), one obtains

$$B_0 = \sigma - \sum_{j=1}^{\infty} B_j \cos(j\bar{\omega}t) - \sum_{j=1}^{\infty} D_j \sin(j\bar{\omega}t). \tag{35}$$

By substituting of (35) in (34), one derives

$$\varepsilon = \frac{\sigma}{E} - \frac{1}{E}\left[\sum_{j=1}^{\infty} B_j \cos(j\bar{\omega}t) + \sum_{j=1}^{\infty} D_j \sin(j\bar{\omega}t) \right] + \sum_{j=1}^{\infty} P_j \cos(j\bar{\omega}t) + \sum_{j=1}^{\infty} R_j \sin(j\bar{\omega}t). \tag{36}$$

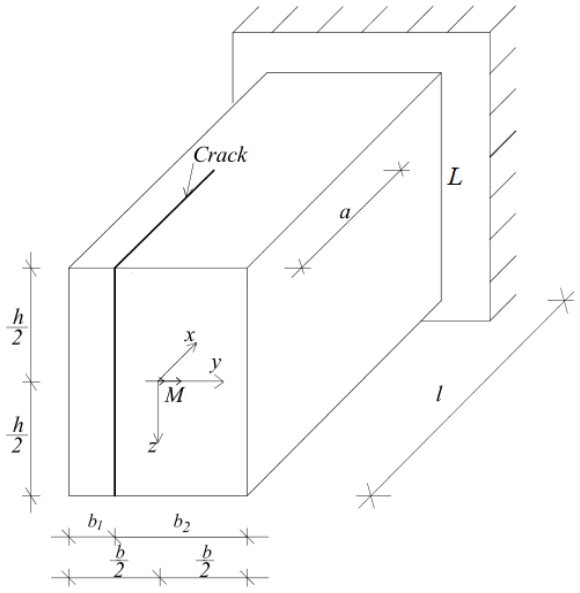

Fig. 3. Viscoelastic beam with a longitudinal crack.

The present paper analyzes the longitudinal fracture in the inhomogeneous (functionally graded) linear viscoelastic beam structure depicted in Fig. 3. Relationship (36) is applied for treating the linear viscoelastic mechanical behaviour of the beam. The beam has the cross-section of a rectangle, b by h. The length of the beam is l. The beam is clamped in section, L. There is a longitudinal crack of length, a, in the beam. The left-hand and right-hand crack arms have width, b_1 and b_2, respectively. The beam is loaded by a bending moment, M, applied at the free end of the right-hand crack arm as shown in Fig. 3. Thus, the left-hand crack arm is stress free. The bending moment varies periodically with time. At $t_i \le t \le t_i + T_\alpha$ the bending moment is M_d. When t is in the interval $[t_i + T_\alpha; t_i + T_\alpha + T_\beta]$ the bending moment is equal to M_g where $M_g = gM_d$.

The beam is made of linearly viscoelastic material that is continuously inhomogeneous along the thickness. The modulus of elasticity and the coefficient of viscosity vary along the thickness of the beam according to the following laws:

$$E = E_q e^{r\frac{\frac{h}{2}+z}{h}}, \tag{37}$$

$$\eta = \eta_q e^{s\frac{\frac{h}{2}+z}{h}}, \tag{38}$$

where

$$-\frac{h}{2} \le z \le \frac{h}{2}. \tag{39}$$

In formulae (37), (38) and (39), z is the vertical centric axis (Fig. 3), E_q and η_q are the values of E and η in the upper surface of the beam, respectively. The parameters, r and s, govern the variation of E and η along the thickness, respectively.

The balance of the energy is analyzed in order to derive the strain energy release rate, G, for the longitudinal crack in the beam (Fig. 3). For this purpose, first, the strain energy, U, in the beam and the angle of rotation, ϕ, of the free end of the right-hand crack arm are determined.

The strain energy is found by integrating of the strain energy density in the right-hand crack arm and in the un-cracked part, $a \le x \le l$, of the beam (the strain energy in the left-hand crack arm is zero since this crack arm is stress free). The strain energy density, u_{01}, in the right-hand crack arm is found as

$$u_{01} = \frac{1}{2}\sigma\varepsilon. \tag{40}$$

By substituting of (36) in (40), one obtains

$$u_{01} = \frac{\sigma^2}{E} - \frac{\sigma}{E}\left[\sum_{j=1}^{\infty} B_j \cos(j\bar{\omega}t) + \sum_{j=1}^{\infty} D_j \sin(j\bar{\omega}t)\right] + \sum_{j=1}^{\infty} P_j \cos(j\bar{\omega}t) + \sum_{j=1}^{\infty} R_j \sin(j\bar{\omega}t). \tag{41}$$

By using of (36), one derives

$$\sigma = E\varepsilon + \left[\sum_{j=1}^{\infty} B_j \cos(j\bar{\omega}t) + \sum_{j=1}^{\infty} D_j \sin(j\bar{\omega}t)\right] + \sum_{j=1}^{\infty} P_j \cos(j\bar{\omega}t) + \sum_{j=1}^{\infty} R_j \sin(j\bar{\omega}t). \tag{42}$$

The distribution of ε along the thickness of the right-hand crack arm is written as

$$\varepsilon = \kappa_1 (z_1 - z_{1n}), \tag{43}$$

where

$$-\frac{h}{2} \le z_1 \le \frac{h}{2}. \tag{44}$$

In formulae (43) and (44), z_1 is the vertical centric axis of the right-hand crack arm, κ_1 and z_{1n} are the curvature and the coordinate of the neutral axis, respectively. By substituting of (43) in (42), the stress is found as

$$\sigma = E\kappa_1 (z_1 - z_{1n}) + \left[\sum_{j=1}^{\infty} B_j \cos(j\bar{\omega}t) + \sum_{j=1}^{\infty} D_j \sin(j\bar{\omega}t)\right] + \sum_{j=1}^{\infty} P_j \cos(j\bar{\omega}t) + \sum_{j=1}^{\infty} R_j \sin(j\bar{\omega}t). \tag{45}$$

The curvature and the coordinate of the neutral axis are determined by using the following equations of equilibrium:

$$N = b_2 \int_{-\frac{h}{2}}^{\frac{h}{2}} \sigma dz_1, \tag{46}$$

$$M = b_2 \int_{-\frac{h}{2}}^{\frac{h}{2}} \sigma z_1 dz_1, \tag{47}$$

where N is the axial force. It is clear that $N = 0$ (Fig. 3). After substituting of the stress in (46) and (47), the two equations are solved with respect to κ_1 and z_{1n} by the MatLab computer program.

The strain energy, U_1, in the right-hand crack arm is found as

$$U_1 = ab_2 \int_{-\frac{h}{2}}^{\frac{h}{2}} u_{01} dz_1 . \tag{48}$$

In order to obtain the strain energy, U_2, in the un-cracked part of the beam, a, b_2 and u_{01} are replaced with $(l-a)$, b and u_{02} in (48). Here, u_{02} is the strain energy density in the un-cracked part of the beam. The stress, σ, is replaced with σ_{uc} in (41) to obtain u_{02}. The quantities, κ_1 and z_{1n}, are replaced with κ_2 and z_{2n} in (45) to derive the stress in the un-cracked beam portion, σ_{uc}. The stress, σ, is replaced with σ_{uc} in equations (46) and (47) which are used to determine κ_2 and z_{2n}.

The strain energy in the beam is found as

$$U = U_1 + U_2 . \tag{49}$$

The angle of rotation of the free end of the right-hand crack arm is written as

$$\phi = \kappa_1 a + \kappa_2 (l-a) . \tag{50}$$

Formula (50) is obtained by using the integrals of Maxwell-Mohr. The balance of the energy is expressed as

$$M\delta\phi = \frac{\Delta U}{\Delta a}\delta a + Gh\delta a \ . \tag{51}$$

From (51), G is found as

$$G = \frac{M}{h}\frac{\partial \phi}{\partial a} - \frac{1}{h}\frac{\partial U}{\partial a} . \tag{52}$$

The strain energy release rate is derived by combining of (48), (49), (50) and (52). The result is

$$G = \frac{M}{h}(\kappa_1 - \kappa_2) - \frac{1}{h}\left(b_2 \int_{-\frac{h}{2}}^{\frac{h}{2}} u_{01} dz_1 - b \int_{-\frac{h}{2}}^{\frac{h}{2}} u_{02} dz_2 \right) . \tag{53}$$

The MatLab computer program is used to solve the integrals in (53).

Another solution of the strain energy release rate is found by applying the method of compliance for verification of (52). For this purpose, first, the compliance, C, of the beam in Fig. 3 is obtained as

$$C = \frac{\phi}{M} . \tag{54}$$

By substituting of (50) in (54), the compliance is derived as

$$C = \frac{1}{M}\left[\ \kappa_1 a + \kappa_2 (l-a) \ \right] . \tag{55}$$

By using the compliance, the strain energy release rate is found as

$$G = \frac{M^2}{2h}\frac{dC}{da} . \tag{56}$$

The compliance (55) is substituted in (56). The result is

$$G = \frac{M}{2h}(\kappa_1 - \kappa_2) . \tag{57}$$

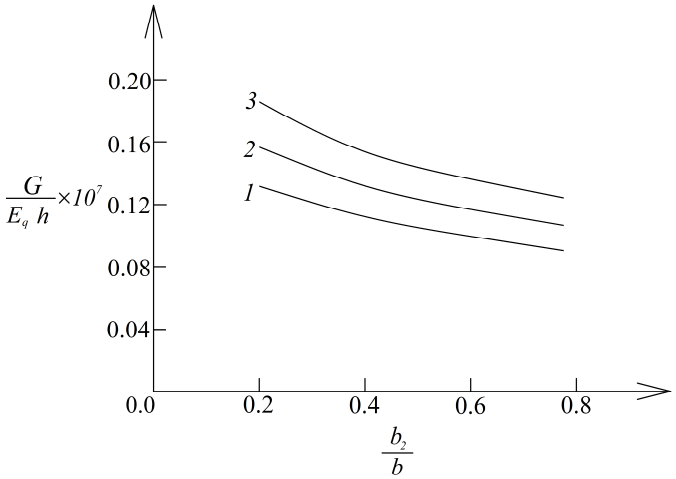

Fig. 4. Plot of non-dimensional strain energy release rate versus b_2/b ratio (curve 1 – at g = 0.5, curve 2 – at g = 1.5 and curve 3 – at g = 2.5).

The strain energy release rates calculated by (57) are exact matches of these obtained by (53). This is verification for the correctness of the solutions. Besides the calculations, it can also be shown theoretically that (57) matches (53). For this purpose, (57) is re-written as

$$G=\frac{M}{h}(\kappa_1-\kappa_2)-\frac{M}{2h}(\kappa_1-\kappa_2)\ . \tag{58}$$

From (58), one obtains

$$G=\frac{M}{h}(\kappa_1-\kappa_2)-\frac{1}{h}\left(\frac{M}{2}\kappa_1-\frac{M}{2}\kappa_2\right). \tag{59}$$

The moment, M, in the second and third terms of the right-hand side of (59) is presented as

$$M=b_2\int_{-\frac{h}{2}}^{\frac{h}{2}}\sigma z_1 dz_1 \tag{60}$$

and

$$M=b\int_{-\frac{h}{2}}^{\frac{h}{2}}\sigma_{uc}z_2 dz_2\ , \tag{61}$$

respectively. Then, (60) and (61) are substituted in (59)

$$G=\frac{M}{h}(\kappa_1-\kappa_2)-\frac{1}{h}\left(b_2\int_{-\frac{h}{2}}^{\frac{h}{2}}\frac{\sigma z_1\kappa_1}{2}dz_1-b\int_{-\frac{h}{2}}^{\frac{h}{2}}\frac{\sigma_{uc}z_2\kappa_2}{2}dz_2\right), \tag{62}$$

Since expressions, $\sigma z_1\kappa_1/2$ and $\sigma_{uc}z_2\kappa_2/2$, are equal to u_{01} and u_{02}, formula (62) is presented as

$$G=\frac{M}{h}(\kappa_1-\kappa_2)-\frac{1}{h}\left(b_2\int_{-\frac{h}{2}}^{\frac{h}{2}}u_{01}dz_1-b\int_{-\frac{h}{2}}^{\frac{h}{2}}u_{02}dz_2\right), \tag{63}$$

which is exact match of (53).

3. Numerical Results

The numerical results found by applying the solutions of the strain energy release rate are presented here in graphical form. The following data are used: $b=0.015$ m, $h=0.0225$ m, $M_d=4$ Nm and $T=80$ s.

If we calculate the strain energy release rate at various b_2/b ratios for three values of the parameter, g, we obtain the plots depicted in Fig. 4. The b_2/b ratio shows the position of the longitudinal crack along the width of the beam.

The strain energy release rate in Fig. 4 is expressed in non-dimensional form as $G_N=G/\left(E_q h\right)$. The plots in Fig. 4 clearly indicate that when the parameter, g, increases, the strain energy release rate increases too. The explanation of this finding consists in the fact that the value of the bending moment, M_g, increases with increasing of the parameter, g. From plots in Fig. 4, it is clear also that when the b_2/b ratio increases, the strain energy release rate decreases (the cause for this behaviour is the fact that the stiffness of the right-hand crack arm increases with increasing of b_2/b ratio).

The plots depicted in Fig. 5 are obtained by calculating of the strain energy release rate at various values of the parameter, r, for three values of the parameter, f. The value of the parameter, g, is 2. From Fig. 5, it can be concluded that the strain energy release rate decreases when the parameter, r, increases. The explanation of this behaviour is in the fact that when the parameter, r, increases, the stiffness of the beam increases too. The plots in Fig. 5 show also that the strain energy release rate decreases with increasing of the parameter, f. This finding can be explained in the following manner. At $g>1$ the bending moment, M_g, is higher than M_d.

Therefore, by increasing of f we decrease the interval of time, T_β, during which the bending moment is equal to its higher value, M_g, and increase the interval of time, T_α, in the course of which the bending moment is equal to its lower value, M_d.

The influence of the parameter, f, on the strain energy release rate is studied also at $g=0.5$.

For this purpose, by performing calculations of the strain energy release rate for three values of f at various h/b ratios, we obtain the plot in Fig. 6. This plot reveals that at $g=0.5$ the strain energy release rate increases with increasing of the parameter, f, which is due to increase of the interval of time, T_α, in which the bending moment is equal to its higher value M_d (when $g<1$, $M_d>M_g$).

The plot in Fig. 6 indicates also the when h/b ratio increases, the strain energy release rate decreases.

Calculations of the strain energy release rate are carried-out also at various values of the parameter, s, for three values of the moment, M_d. The results of these calculations are used to obtain the plots depicted in Fig. 7. It is obvious from Fig. 7 that when the parameter, s, increases, the strain energy release rate decreases (this is caused by increase of the beam stiffness). From the plots in Fig. 6, we found also that with increasing of M_d, the strain energy release rate increases too.

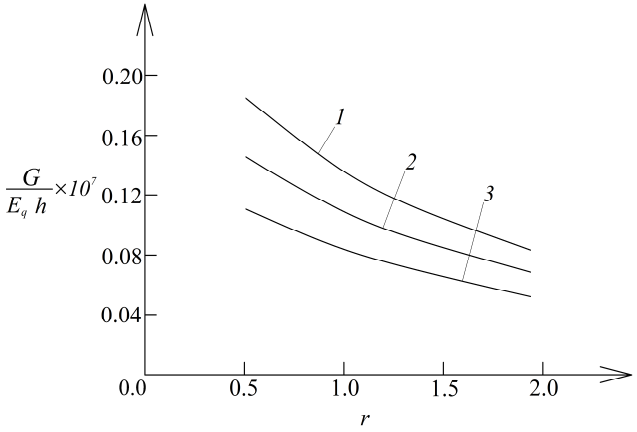

Fig. 5. Plot of non-dimensional strain energy release rate versus parameter r (curve 1 – at $f = 0.2$, curve 2 – at $f = 0.4$ and curve 3 – at $f = 0.6$).

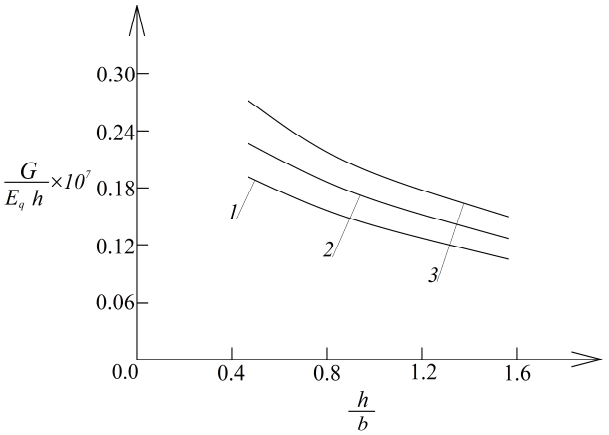

Fig. 6. Plot of non-dimensional strain energy release rate versus h/b ratio (curve 1 – at $f = 0.2$, curve 2 – at $f = 0.4$ and curve 3 – at $f = 0.6$).

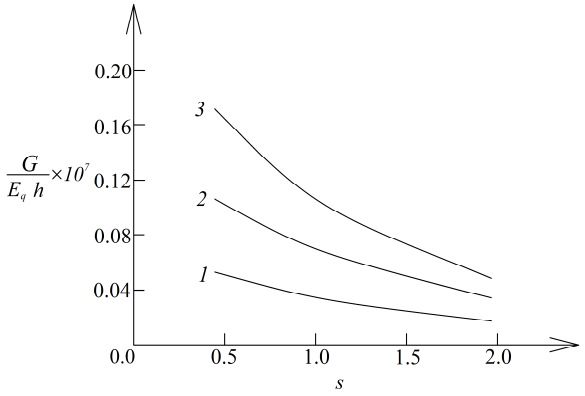

Fig. 7. Plot of non-dimensional strain energy release rate vs. parameter s (curve 1 – at $M_d = 2$ Nm, curve 2 – at $M_d = 3$ Nm and curve 3 – at $M_d = 4$ Nm).

4. Conclusion

The effects of periodic loading on longitudinal fracture in a linear viscoelastic beam structure were studied. The beam under consideration was subjected to bending by a moment applied at the free end of the right-hand crack arm. The moment varied periodically with time. The beam was made of viscoelastic material that is continuously inhomogeneous (functionally graded) along the thickness. The modulus of elasticity and the coefficient of viscosity varied smoothly along the thickness of the beam. A solution of the strain energy release rate that accounts for the viscoelastic mechanical behaviour of the inhomogeneous beam and for the periodic character of the external loading was derived by considering the balance of the energy. A solution was obtained also by considering the compliance of the beam under periodic loading for verification. The analysis performed indicated that when the parameter, g, increases, the strain energy release rate increases too. With increasing of b_2/b ratio, the strain energy release rate decreases. The strain energy release rate decreases also with increasing of the parameter, f, at $g > 1$. When $g < 1$, however, the strain energy release rate increases with increasing of the parameter, f. It was also found that if the parameter, s, increases, the strain energy release rate decreases. From view point of practical engineering, one of the important applications of this paper is that the theoretical derivations can be used to determine the durability of the structure. Since the beam structure under consideration exhibited viscoelastic behaviour, the durability can be defined as the value of time at which the crack will start to grow. In order to determine the durability, the strain energy release rate has to be obtained by using the theoretical derivations at various values of time and compared to the critical strain energy release rate (known as fracture toughness). The value of time at which the strain energy release rate becomes equal to the fracture toughness is the durability of the viscoelastic functionally graded structure under periodic loading.

Author Contributions

Not applicable.

Acknowledgments

Not applicable.

Conflict of Interest

The author declared no potential conflicts of interest with respect to the research, authorship, and publication of this article.

Funding

The author received no financial support for the research, authorship, and publication of this article.

Data Availability Statements

The datasets generated and/or analyzed during the current study are available from the corresponding author on reasonable request.

References

[1] Markworth, A.J., Ramesh, K.S., Parks, Jr.W.P., Review: modeling studies applied to functionally graded materials, *J. Mater. Sci.*, 30(3), 1995, 2183-2193.
[2] Butcher, R.J., Rousseau, C.E., Tippur, H.V., A functionally graded particulate composite: Measurements and Failure Analysis, *Acta. Mater.*, 47(2), 1999, 259-268.
[3] Hirai, T., Chen, L., Recent and prospective development of functionally graded materials in Japan, *Mater Sci. Forum*, 308-311(4), 1999, 509-514.
[4] Miyamoto, Y., Kaysser, W.A., Rabin, B.H., Kawasaki, A., Ford, R.G., *Functionally Graded Materials: Design*, Processing and Applications, Kluwer Academic Publishers, Dordrecht/London/Boston, 1999.
[5] Han, X., Xu, Y.G., Lam, K.Y., Material characterization of functionally graded material by means of elastic waves and a progressive-learning neural network, *Compos. Sci. Technol.*, 61(10), 2001, 1401-1411.
[6] Gasik, M.M., Functionally graded materials: bulk processing techniques, *Int. J. Mater. Prod. Technol.*, 39(1-2), 2010, 20-29.
[7] Nemat-Allal, M.M., Ata, M.H., Bayoumi, M.R., Khair-Eldeen, W., Powder metallurgical fabrication and microstructural investigations of Aluminum/Steel functionally graded material, *Mater. Sci. Appl.*, 2(5), 2011, 1708-1718.
[8] Shrikantha Rao, S., Gangadharan, K.V., Functionally graded composite materials: an overview, *Proc. Mater. Sci.*, 5(1), 2014, 1291-1299.
[9] Wu, X.L., Jiang, P., Chen, L., Zhang, J.F., Yuan, F.P., Zhu, Y.T., Synergetic strengthening by gradient structure, *Mater. Res. Lett.*, 2(1), 2014, 185–191.
[10] Arefi, M., Rahimi, G.H., Nonlinear analysis of a functionally graded beam with variable thickness, *Sci. Res. Essays*, 8(6), 2013, 256-264.
[11] Arefi, M., Nonlinear analysis of a functionally graded beam resting on the elastic nonlinear foundation, *J. Theor. Appl. Mech.*, 44(2), 2014, 71-82.
[12] Arefi, M., Elastic solution of a curved beam made of functionally graded materials with different cross section, *Steel Compos. Struct.*, 18(3), 2015, 659-672.
[13] Saiyathibrahim, A., Subramaniyan, R. Dhanapl, P., *Centrefugally cast functionally graded materials – review*, In: International Conference on Systems, Science, Control, Communications, Engineering and Technology, 2016.
[14] Mahamood, R.M., Akinlabi, E.T., *Functionally Graded Materials*, Springer, 2017.
[15] Dolgov, N.A., Effect of the elastic modulus of a coating on the serviceability of the substrate-coating system, *Strength Mater.*, 37(2), 2002, 422-431.
[16] Dolgov, N.A., Determination of Stresses in a Two-Layer Coating, *Strength Mater.*, 37(2), 2005, 422-431.
[17] Dolgov, N.A., Analytical Methods to Determine the Stress State in the Substrate–Coating System Under Mechanical Loads, *Strength Mater.*, 48(1), 2016, 658-667.
[18] Rizov, V.I., Influence of the viscoelastic material behaviour on the delamination in multilayered beam, *Procedia Struct. Integr.*, 25, 2020, 88-100.
[19] Rizov, V.I., Longitudinal fracture analysis of continuously inhomogeneous beam in torsion with stress relaxation, *Procedia Struct. Integr.*, 28, 2020, 1212-122.
[20] Rizov, V.I., Continuously inhomogeneous beam structure with creep: a longitudinal crack study, *Struct. Monit. Maint.*, 8(1), 2021, 111-124.

ORCID iD

Victor Rizov https://orcid.org/0000-0002-0259-3984

How to cite this article: Rizov V. Effects of Periodic Loading on Longitudinal Fracture in Viscoelastic Functionally Graded Beam Structures, *J. Appl. Comput. Mech.*, 8(1), 2022, 370–378. https://doi.org/10.22055/JACM.2021.37953.3141